Optics Letters

Use of dyes to increase phase contrast for biological holographic microscopy

JAY L. NADEAU,[1,*] YONG BIN CHO,[1] AND CHRISTIAN A. LINDENSMITH[2]

[1]Graduate Aerospace Laboratories, Division of Engineering & Applied Sciences, California Institute of Technology, 1200 E. California Blvd., Pasadena, California 91125, USA
[2]Jet Propulsion Laboratory, California Institute of Technology, 4800 Oak Grove Dr., Pasadena, California 91109, USA
*Corresponding author: jnadeau@caltech.edu

Holographic microscopy is an emerging biological technique that provides amplitude and quantitative phase imaging, though the contrast provided by many cell types and organelles is low, and until now no dyes were known that increased contrast. Here we show that the metallocorrole Ga(tpfc)(SO₃H)₂, which has a strong Soret band absorption, increases contrast in both amplitude and phase and facilitates tracking of _Escherichia coli_ with minimal toxicity. The change in phase contrast may be calculated from the dye-absorbance spectrum using the Kramers–Kronig relations, and represents a general principle that may be applied to any dye or cell type. This enables the use of holographic microscopy for all applications in which specific labeling is desired. © 2015 Optical Society of America

Ga(tpfc)(SO₃H)₂ — *(see note: rendered as $\mathrm{Ga(tpfc)(SO_3H)_2}$)*

Digital holographic microscopy (DHM) is a technique where an object beam, after interacting with a sample, combines with a reference beam to encode both the amplitude and phase of the light as an interference pattern (hologram) that is recorded. The hologram can be used to numerically reconstruct the object beam at any location in the sample volume [1–4]. The advantages of this technique are that focusing is performed digitally, after the fact, and that each plane in a three-dimensional sample volume is probed simultaneously (albeit not as individual planes, but as a single image, which imposes limits on the density of the sample as we have explored with bacterial cultures [4]). Amplitude images correspond to those seen with brightfield-transmission light microscopy, while phase images have no direct counterpart in light microscopy, though they may be used to construct darkfield or phase contrast-like images. For example, a DHM DIC (differential interference contrast) image may be obtained by taking the derivative of the image along the x direction; the resulting images are comparable to Nomarski DIC [6]. The appearance of biological objects in amplitude and phase is very different, with some cell types essentially transparent

under amplitude but highly visible in phase, or *vice versa* [4] [Figs. 1(A) and 1(B)]. The contrast in phase images at a point x, y is provided by the spatially averaged phase difference $\Delta \varphi$, which is related to the difference in indices of refraction between the medium (n_m) and cell (n_c) [5]:

$$\Delta \varphi = \frac{2\pi}{\lambda} h(x, y)[n_c(x, y) - n_m], \tag{1}$$

where λ is the wavelength of the illuminating light, and h is the thickness of the cell at the measured point; n_c represents a z-integrated value at that same point and thus also depends upon cell structure.

DHM phase imaging is extremely sensitive to small changes in the index of refraction, which can occur in healthy or diseased cells as a result of ion channel function, pre-apoptotic changes, or osmotic shock: primarily changes that affect cell volume [6–10]. Some groups have reported that changes of 4×10^{-4} in refractive index may be resolved using typical off-axis DHM configurations; however, such experiments require very careful phase monitoring and background correction, and cannot be seen by eye [5].

Until now, such imaging has only been performed as a label-free technique, or by increasing phase contrast by immersion of the sample into a high-index medium such as glycerol. Labeling of cells with typical colorimetric or fluorescent dyes such as fluorescein or green fluorescent protein (GFP) does not change their refractive index and therefore does not improve phase contrast. However, there are conditions under which labeling is desirable. DHM is an important emerging technique for tracking three-dimensional motility of microorganisms. It has so far been restricted almost entirely to eukaryotes such as algae and diatoms [11]; one paper has reported extensive development of de-noising algorithms in order to identify bacteria [12]. There are several reasons why imaging bacteria with DHM is challenging. The first is the small size of the cells (usually 1–2 μm); few instruments have been reported with the required spatial resolution. Bacteria also tend to be nearly invisible in both amplitude and phase. *Escherichia coli* has been reported to have a refractive index of ∼1.384 [13], differing from water only at the second decimal place (imaging is performed in water or in dilute saline, $n = 1.33$). The combination of small size and small refractive-index change results in both terms in Eq. (1) being small, and
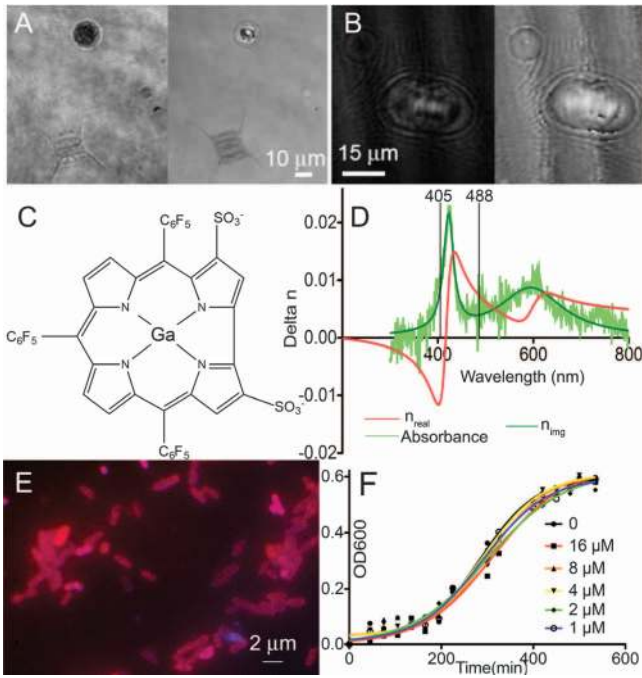
Fig. 1. Principles of phase imaging and increased contrast. (A) Untreated pond water sample in amplitude (left) and phase (right) showing a photosynthetic algal cell (round) and a nonphotosynthetic diatom. (B) Cultured *Paramecium micromultinucleatum* cell in intensity (left) and phase (right). (C) Structure of Ga(tpfc)(SO$_3$H)$_2$. (D) Measured change in absorbance spectrum of cells incubated with 4-μM dye (light green), with fit to a sum of 2 Lorentzians designated as the function n_{img} (dark green) and the resulting predicted change in the real part of the refractive index, n_{real} (red). (E) Fluorescence of *E. coli* incubated with 4-μM dye. (F) Growth curves showing optical density at 600 nm (OD600) versus time for concentrations of dye up to 16 μM with curves indicating fits as given in the text.

thus very low contrast. Being able to increase the contrast in phase imaging would permit automated detection and tracking and thus facilitate motility studies of this and other organisms. A nontoxic dye that does not affect medium viscosity is necessary in order to preserve native motility.

Previous work has related changes in absorbance spectrum of dyed microspheres or cells to changes in index of refraction [14–15]. The difference in absorbance spectrum between the dyed and undyed cells is directly related to the imaginary part of the index of refraction, n_{img}. The change in real part n_{real} can then be calculated using the Kramers–Kronig relation, which may be expressed as a function of wavelength as

$$n_{real}(\lambda) = \frac{-2\lambda^2}{\pi} \mathcal{P} \int_{\delta}^{\infty} \frac{n_{img}(\lambda')}{\lambda'(\lambda'^2 - \lambda^2)} \, d\lambda', \tag{2}$$

where $\mathcal{P}$ represents the Cauchy principal value, and the value δ is included to avoid divergence at $\lambda = 0$. Since the refractive index change is an integral over the absorption, the greatest increase in n will be seen at wavelengths greater than the principal absorbance peak. The peak increase in RI will occur at approximately the highest slope of the absorption curve. Since spatial resolution is diffraction limited in direct proportion to the illumination wavelength, the key for bacterial imaging is to choose a dye with a strong ultraviolet to blue absorbance,

and perform imaging using blue to green illumination (avoiding the ultraviolet so as so prevent cell damage). Laser diodes in this range include 405 nm (violet), 450, 473, and 488 nm.

Corroles are aryl-substituted corrin derivatives that have similar physicochemical properties to porphyrins, such as the ability to chelate metal ions and the presence of a strong blue-violet Soret band absorption. The Soret band results from $\pi - \pi^*$ transitions, and extinction coefficients at this peak can be $>10^5$ M^{-1} cm^{-1} [16–18]. Both porphyrins and corroles are commonly used as photosensitizers; in the absence of targeted illumination, they usually show little cytotoxicity [19–21]. Additionally, gram-negative bacteria are resistant to many photosensitizers [22]. In this work, we labeled *Escherischia coli* (AW405) cells with a metallocorrole, Ga(tpfc)(SO$_3$H)$_2$ [Fig. 1(C)]. This sulfonic acid-substituted dye binds tightly to proteins and has been shown to be readily internalized by several cancer cell lines [23].

Absorption spectroscopy (using a Varian Cary 50) was used to measure the spectrum of the dye and of bacteria incubated with and without dye. The change in index of refraction of bacteria with 0.4-μM dye added was estimated by evaluating Eq. (2) using Mathematica 10 [Fig. 1(D)]. The bulk change in index at the dye absorbance peak was ~0.015, corresponding to 1% of the real index, consistent with previous results [14,17]. A decrease in index was expected at 405 nm, as can be seen in the figure. These changes are significantly larger than what is seen due to natural variations in cell volume and thickness.

For imaging, dye was added to cells in 0.9% NaCl at mid-log phase at several concentrations (0.2–4 μM) and allowed to incubate for a minimum of 30–60 min to permit uptake. Before imaging, cells were pelleted by centrifugation at 3000 × g and resuspended in "motility medium" (10 mM potassium phosphate, 10 mM NaCl, 0.1 mM EDTA, 0.1 mM glucose, pH 7.0). Under widefield fluorescence microscopy, the dye was shown to strongly label a significant fraction of cells even at sub-micromolar concentrations; many of the most intensely fluorescent cells were elongated. At 4 μM, nearly all cells were labeled [Fig. 1(E)]. Cells remained fluorescent for at least 48 h post labeling.

Dye was added to *E. coli* cells in lysogeny broth (LB) for toxicity testing. Dye was added at lag phase, and bacterial growth monitored until decline by measuring optical density at 600 nm (OD600) on a Sequoia-Turner Model 340 spectrophotometer. Under ordinary room light, the dye showed minimal toxicity even at the highest concentration tested, with statistically insignificant changes in exponential growth and stationary-phase density [Fig. 1(F)]. Growth curves were fit to a Boltzmann sigmoid with R > 0.99. The equation is

$$y = \frac{K}{1 + \exp\left(\frac{V_{50} - t}{m}\right)}, \tag{3}$$

with the values ± standard errors as follows: $K = 0.60 \pm 0.02$ for all concentrations; $V_{50} = 287 \pm 9$, 290 ± 9, 300 ± 13, 292 ± 7, 304 ± 9, 312 ± 10; and $m = 60 \pm 7$, 70 ± 8, 84 ± 15, 64 ± 7, 64 ± 9, 76 ± 12 for 0, 1, 2, 4, 8, and 16-μM dye, respectively.

We then imaged the cells using a custom off-axis DHM instrument as described previously [24], using laser illumination at either 405 or 488 nm and dye concentrations of 0.2 or 4 μM. For DHM, cells were sandwiched between a slide and coverslip at a density of ~10^6 cells/mL (1/100 dilution of a culture at OD600 = 0.8). When illuminated at 488 nm, labeled cells showed increased phase contrast relative to controls (Fig. 2).

Raw holograms of control and labeled cells are shown in Figs. 2(A) and 2(B) and reconstructed phase images of a single focal plane in Figs. 2(C) and 2(D). Although the cultures were at the same optical density, the dyed sample's hologram showed less contrast because of the greater DC term in the hologram generated by the more strongly absorbing sample. Similarly, the reconstruction appeared to contain more cells because of the increased visibility of the cells across multiple focal planes.

It can be clearly seen in Figs. 2(C) and 2(D) that some cells appeared light and some dark. Examination of time and z-stacks showed "phase flipping"—that is, cells turned from light to dark either in time or in depth in both dyed samples and controls. This is a manifestation of the so-called Gouy-phase anomaly [25,26] as an object passes through the geometric focus. It has been previously described in detail in the context of DHM [27], and used for precise z-localization of weakly scattering objects for tracking [28]. The dye-labeled cells showed more rapid phase shifts as well as magnified contrast, because the effective contrast difference was doubled as the cells shifted from light to dark. In order to capture most cells, both light and dark, a maximum intensity z-projection across the depth of the sample could be used. A simple thresholding algorithm applied to a single plane failed to separate the control cells from the noise caused by out-of-focus cells appearing as Airy rings; the same thresholding algorithm was able to identify the dyed cells [Figs. 2(E) and 2(F)]. Correct identification of cells was confirmed by observation of motility in the time series (see Visualization 1, Visualization 2, and Visualization 3 for videos of control cells, cells with 0.2-µM dye, and cells with 4-µM dye).

What is also apparent from the plots is the importance of the parameter h in Eq. (1). Cells viewed end-on showed greater contrast than cells viewed lengthwise. This effect was noticeable in controls, but dramatically enhanced contrast in dyed cells. E. coli cells have a mean size of 0.8×2 µm, so a single cell end-on will show a 2.5-fold increased contrast relative to a cell lengthwise. Figures 3(A) and 3(B) show z-stacks through end-on cells, with phase flipping in both the control and the dyed sample. Phase shifts were useful not only for determining focus, but also for studies of motility. Since E. coli (and similar enteric strains) change direction by tumbling, the ability to rapidly detect tumbling events is useful for automated classification of trajectories. In control cells, a small increase in intensity was seen as the cells turned end-on (Visualization 4). In the labeled samples, the change was more intense, and phase reversals were nearly always observed (Visualization 5).

Figures 3(C) and 3(D) show z-stacks through lengthwise cells, indicating the dramatic increase in contrast to the dyed sample and the visibility of the cell over an increased number of focal planes. In the controls, the lengthwise cells were difficult to separate from background.

Figure 3(E) shows the signal strength over background for representative cells in the plane of their best focus. The dye increased signal-to-noise in end-on cells by approximately a factor of 2, and in lengthwise cells by more than a factor of 3; this difference is due to the approximately 2-fold greater thickness of the end-on cells. Figure 3(F) shows the strength of the signal over the mean background noise versus depth for selected cells seen end-on and lengthwise. It can be appreciated from these plots that the cells stained with the corrole were visible above the noise at significantly more depths than the controls. The magnitude of the light-to-dark reversals seen in dyed cells was also significantly greater than in controls. Both
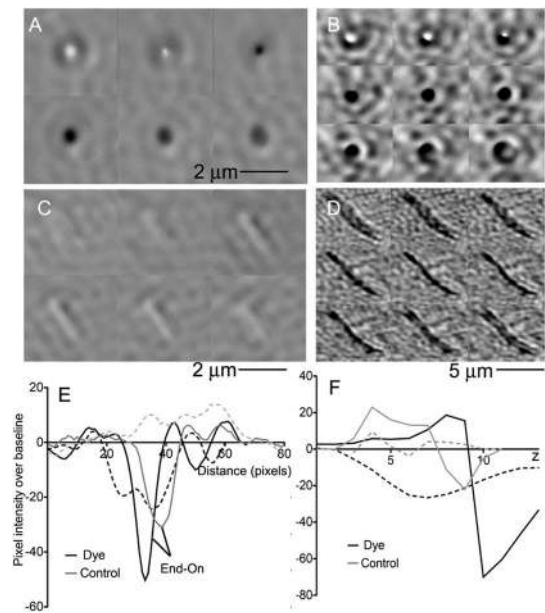
Fig. 3. Phase flipping and thickness dependence. (A) Stack through 6 z-planes of an unlabeled cell oriented end-on (Visualization 4). (B) Stack through 9 z-planes of a labeled cell oriented end-on (Visualization 5). (C) Stack through 6 z-planes of an unlabeled cell oriented lengthwise. (D) Stack through 9 z-planes of a labeled cell oriented lengthwise. (E) Signal over background in a single z-plane of a selected unlabeled cell oriented lengthwise (dashed gray line) and a cell oriented end-on (solid gray line) compared with a dyed cell oriented lengthwise (dashed black line) and dyed cell end-on (solid black line). (F) Visibility of cells through multiple z-planes. Gray, dashed: control lengthwise; gray, solid: control end-on; black, dashed: dyed lengthwise; black, solid: dyed end-on. (In both images and graphs, each z-plane corresponds to ~2 µm.)
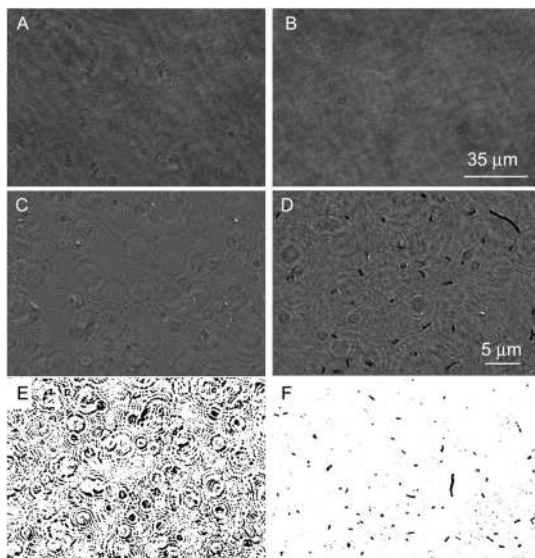

Fig. 2. Phase images of E. coli with and without corrole labeling. (A) Raw hologram, unlabeled. (B) Raw hologram, dyed. (C) Single-plane reconstruction of unlabeled cells (Visualization 1). (D) Single-plane phase reconstruction of labeled cells (Visualization 2, Visualization 3). (E) and (F) Application of simple thresholding algorithm to (E) unlabeled and (F) labeled cells.

of these features facilitate automated feature detection and tracking, and reduce the number of fragmented tracks, which will be the topic of our future work. For thresholding and tracking, phase reversals may be eliminated by taking the square root of the square of the image after subtracting the mean to convert the unsigned 8-bit number to a signed number.

These effects were seen only at 488-nm illumination. When illuminated at 405 nm, labeled cells showed decreased contrast over control cells with a brighter background, as expected from Fig. 1(B) (not shown).

Dye-labeled cells also showed moderate increases in amplitude contrast at absorption peak (Fig. 4). At 488 nm, both the control and dye showed the same intensity contrast, with a signal-to-noise value of approximately 3 [Figs. 4(A)–4(C)]. At 405 nm, the signal-to-noise in control cells was reduced to ~2, with cells difficult to detect by eye. Cells labeled with the corrole showed a signal-to-noise of ~4 with substantially increased contrast [Figs. 4(D)–4(F)]. This increased amplitude signal was similar to what we have previously observed in cells containing chlorophyll, which has an extinction coefficient of ~10^5 at 405 nm [4].

This Letter introduces a general principle that may be used to create phase contrast for any quantitative phase-imaging applications. For longer illumination wavelengths, such as the commonly used 633 nm, some index change might be seen with standard colorimetric dyes. However, for 488-nm illumination, the corroles and porphyrins represent a special class of molecules with very strong absorption in the blue-to-violet range, which is ideal for imaging bacteria. It is important to note that the dye fluorescence is unnecessary and in fact may create increased background. The ideal dye for these applications would thus be highly absorptive without emitting fluorescence, or would be illuminated so far off peak as to emit negligible fluorescence. The design of probes for holographic imaging is in its infancy, but promises to make this technique of general applicability to a wide range of biological problems, particularly those where instantaneous three-dimensional snapshots of dynamic processes are desired.

In conclusion, contrast in phase imaging may be augmented by using dyes that increase the index of refraction, of which corroles are an example at 488-nm excitation. Quantitative

phase imaging is therefore a technique amenable to specific labeling. Other classes of dyes, particularly porphyrins, show similar spectra and are expected to work as well. The techniques for labeling bacterial cells may be extended to more complex cells and organisms and facilitate labeling of specific organelles and structures. For example, the molecule used in this Letter accumulates in the nuclei of certain cancer cells but not others, indicating in which cancers it may be used as a drug carrier [23]. This accumulation should be observable by DHM.

REFERENCES

1. P. Ferraro, S. De Nicola, A. Finizio, G. Coppola, S. Grilli, C. Magro, and G. Pierattini, Appl. Opt. **42**, 1938 (2003).
2. F. Dubois, M. L. Requena, C. Minetti, O. Monnom, and E. Istasse, Appl. Opt. **43**, 1131 (2004).
3. P. Marquet, B. Rappaz, P. J. Magistretti, E. Cuche, Y. Emery, T. Colomb, and C. Depeursinge, Opt. Lett. **30**, 468 (2005).
4. J. Kuhn, B. Niraula, K. Liewer, J. K. Wallace, E. Serabyn, E. Graff, C. Lindensmith, and J. L. Nadeau, Rev. Sci. Instrum. **85**, 123113 (2014).
5. B. Rappaz, P. Marquet, E. Cuche, Y. Emery, C. Depeursinge, and P. Magistretti, Opt. Express **13**, 9361 (2005).
6. F. Dubois, C. Yourassowsky, O. Monnom, J. C. Legros, O. Debeir, P. Van Ham, R. Kiss, and C. Decaestecker, J. Biomed. Opt. **11**, 054032 (2006).
7. M. Falck Miniotis, A. Mukwaya, and A. Gjorloff Wingren, PLoS One **9**, e106546 (2014).
8. P. Jourdain, N. Pavillon, C. Moratal, D. Boss, B. Rappaz, C. Depeursinge, P. Marquet, and P. J. Magistretti, J. Neurosci. **31**, 11846 (2011).
9. B. Kemper, D. Carl, J. Schnekenburger, I. Bredebusch, M. Schafer, W. Domschke, and G. von Bally, J. Biomed. Opt. **11**, 34005 (2006).
10. B. Rappaz, B. Breton, E. Shaffer, and G. Turcatti, Comb. Chem. High Throughput Screening **17**, 80 (2014).
11. J. Sheng, E. Malkiel, J. Katz, J. Adolf, R. Belas, and A. R. Place, Proc. Natl. Acad. Sci. USA **104**, 17512 (2007).
12. M. Molaei and J. Sheng, Opt. Express **22**, 32119 (2014).
13. A. E. Balaev, K. N. Dvoretski, and V. A. Doubrovski, Proc. SPIE **4707**, 253 (2002).
14. A. K. Gaigalas, S. Choquette, and Y. Zhang, J. Res. Nat. Inst. Stand. Technol. **118**, 15 (2013).
15. B. Rappaz, F. Charriere, C. Depeursinge, P. J. Magistretti, and P. Marquet, Opt. Lett. **33**, 744 (2008).
16. C. Rimington, Biochem. J. **75**, 620 (1960).
17. I. H. Wasbotten, T. Wondimagegn, and A. Ghosh, J. Am. Chem. Soc. **124**, 8104 (2002).
18. J.-L. Soret, Comptes rendus de l'Académie des Sci. **97**, 1269 (1883).
19. R. Bonnett, Chem. Soc. Rev. **24**, 19 (1995).
20. E. D. Sternberg and D. Dolphin, Tetrahedron **54**, 4151 (1998).
21. L. You, H. Shen, L. Shi, G. Zhang, H. Liu, H. Wang, and L. Ji, Sci. China Phys. Mech. Astron. **53**, 1491 (2010).
22. Z. Malik, J. Hanania, and Y. Nitzan, J. Photochem. Photobiol. B Biol. **5**, 281 (1990).
23. P. Lim, A. Mahammed, Z. Okun, I. Saltsman, Z. Gross, H. B. Gray, and J. Termini, Chem. Res. Toxicol. **25**, 400 (2012).
24. J. K. Wallace, S. Rider, E. Serabyn, J. Kuhn, K. Liewer, J. Deming, G. Showalter, C. Lindensmith, and J. L. Nadeau, Opt. Express **23**, 17367 (2015).
25. S. Feng and H. G. Winful, Opt. Lett. **26**, 485 (2001).
26. L. G. Gouy, CR Hebdomadaires Séances Acad. Sci. **110**, 1251 (1890).
27. L. Wilson and R. Zhang, Opt. Express **20**, 16735 (2012).
28. L. G. Wilson, L. M. Carter, and S. E. Reece, Proc. Natl. Acad. Sci. USA **110**, 18769 (2013).
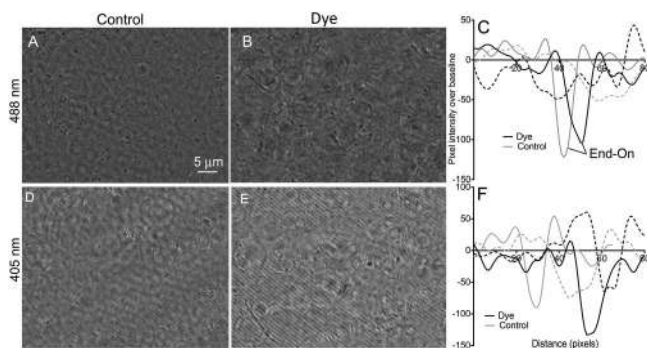
Fig. 4. Amplitude images of control and corrole-labeled *E. coli.* (A), (B) Illumination at 488 nm. (C) Line profiles through selected cells at 488-nm excitation, showing identical signal-to-noise for labeled (black) and unlabeled (gray) cells, both lengthwise and end-on. (D), (E) Illumination at 405 nm. (F) Line profiles through selected cells at 405-nm excitation showing increased signal-to-noise for labeled (black) versus unlabeled (gray) cells.